Design rules, accurate enthalpy prediction, and synthesis of stoichiometric Eu^{3+} quantum memory candidates

Zachary W. Riedel[†,‡] and Daniel P. Shoemaker[*,†,‡]

†*Department of Materials Science and Engineering, University of Illinois Urbana-Champaign, Urbana, Illinois 61801, United States*
‡*Materials Research Laboratory, University of Illinois Urbana-Champaign, Urbana, Illinois 61801, United States*

E-mail: dpshoema@illinois.edu

Abstract

Stoichiometric Eu^{3+} compounds have recently shown promise for building dense, optically addressable quantum memory as the cations' long nuclear spin coherence times and shielded 4f electron optical transitions provide reliable memory platforms. Implementing such a system, though, requires ultra-narrow inhomogeneous linewidth compounds. Finding this rare linewidth behavior within a wide range of potential chemical spaces remains difficult, and while exploratory synthesis is often guided by density functional theory (DFT) calculations, lanthanides' 4f electrons pose unique challenges for stability predictions. Here, we report DFT procedures that reliably reproduce known phase diagrams and that correctly predict two experimentally realized quantum memory candidates. We are the first to synthesize the double perovskite halide Cs_2NaEuF_6. It is an air-stable compound with a calculated band gap of 6.9 eV that surrounds Eu^{3+} with mononuclidic elements, which are desirable for avoiding inhomogeneous linewidth broadening. We also analyze computational database entries to identify phosphates and iodates as the next generation of chemical spaces for stoichiometric quantum memory system studies. This work identifies new candidate platforms for exploring chemical effects on quantum memory candidates' inhomogeneous linewidth while also providing a framework for screening Eu^{3+} compound stability with DFT.

Introduction

Rare-earth cations have up to six-hour hyperfine energy level coherence times and several millisecond optical coherence times because of 4f-4f orbital optical transitions well-shielded by filled 5s and 5p orbitals.[1–4] The long-lived states allow for faithful transfer between optical and spin qubits. Building rare-earth qubits typically involves low dopant concentrations to improve coherence times, but along with low optical density comes site inhomogeneity and reduced efficiency. However, stoichiometric rare-earth materials with drastically higher rare-earth concentrations and improved site homogeneity can reduce inhomogeneous linewidths to the point that transitions involving hyperfine energy levels separated by only ∼70-140 MHz are resolved.[5] Promisingly, $EuCl_3{\cdot}6H_2O$ has demonstrated an ultra-narrow $^5D_0 \rightarrow {}^7F_0$ transition linewidth paired with a near-millisecond coherence time,[6–9] but its environmental instability and needed isotopic enrichment prompt searches for additional candidates.

A desirable candidate would be air stable, have a large europium cation separation to limit

unintended interactions, consist of mononuclidic elements, and have a polar europium site symmetry to allow observation of the narrow $^5D_0 \rightarrow {}^7F_0$ transition. These conditions, along with europium's tendency to be divalent, severely limit the known viable materials that may achieve the desired narrow inhomogeneous linewidth. On the other hand, the chemical similarity of lanthanide elements makes them ideally suited for using known structures as prototypes for building unrealized Eu^{3+} compounds. With prototype structures from material databases, we quickly increase our potential candidate list but with no indication of chemical stability.

Density functional theory (DFT) calculations may, therefore, guide synthesis efforts of the proposed candidates. Still, care must be taken with DFT calculations to handle the high-energy but spatially shielded 4f electrons of europium appropriately. Including 4f electrons in the valence can reduce transferability while increasing the necessary kinetic energy cutoff.[10] Freezing the 4f electrons in the core eliminates these issues and, despite eliminating the magnetic contribution, has shown promise in modeling known lanthanide systems.[11] If 4f electrons are frozen in the core, separate pseudopotentials are needed for divalent ($4f^7$ core) and trivalent ($4f^6$ core) europium. Starting with tests of DFT parameters and a set of proposed candidates, DFT stability calculations can provide a practical number of compounds to explore experimentally.

Computational Methods

Proposing candidates

To limit inhomogeneous broadening from isotope variations, we started with compositions containing Eu^{3+}, one or two mononuclidic cations, and a mononuclidic anion or oxygen. We excluded mononuclidic cations that are magnetic, toxic, radioactive, or in the lanthanides, leaving 12: Al^{3+}, $Au^{+/3+}$, Bi^{3+}, Cs^+, Na^+, Nb^{5+}, $P^{3+/5+}$, Rh^{3+}, Sc^{3+}, and Y^{3+}. We included O^{2-} in addition to the mononuclidic anions F^- and I^- to expand the initial search range. Oxygen should contribute little to broadening because of the high natural abundance of ^{16}O and its low mass relative to the other elements.[9] This process gives 234 ternary and quaternary combinations (eg. Eu^{3+}-Cs^+-Na^+-F^-). Adding quaternary oxyfluorides and iodates brings the total to 258 combinations.

For each chemical combination, we used the pymatgen package[12] to find the most likely ionic substitutions,[13] capping them at 15 per system. We used the default log probability threshold of 0.001, where the false positive rate for substitution in the ICSD[14] test set was near zero and the true positive rate was near 50%.[13] We then collected Materials Project database entries[15,16] for the substituted combinations (eg. Cs_2NaNdF_6 for Nd^{3+}-Cs^+-Na^+-F^-). We substituted the desired ion(s) into these entries and any of their polymorphs.

From the proposed materials, we excluded options where the minimum Eu^{3+} separation for every polymorph was <3.9 Å to avoid unwanted Eu^{3+} cation interactions. We also removed candidates predicted to lie in phase diagrams that were already thoroughly investigated experimentally. These included two fluorides not in published phase diagrams, $CsEu_3F_{10}$ and $NaEu_2F_7$;[17] Eu-Bi-O compositions in a solid-solution phase region[18] or with non-stoichiometric structures;[19] Eu-Y-O compositions expected to be solid-solutions;[20] and Eu-Al-O compounds not appearing in phase diagrams.[21,22]

Pseudopotentials

For structure relaxation, we tested pseudopotentials from the pslibrary set (v. 1.0.0)[10] that allow for spin-orbit coupling contributions and ones from the SSSP Efficiency (v. 1.1.2)[23–25] set that use the scalar relativistic approximation.[26–28] The pslibrary europium pseudopotentials placed the 4f electrons in the core while the SSSP europium pseudopotential placed them in the valence. For dielectric function calculations, Quantum Espresso requires norm-conserving pseudopotentials, so we used pseudopotentials from the Pseudo-Dojo set.[29] Band structures

calculated with the Pseudo-Dojo pseudopotentials matched those calculated with the pslibrary pseudopotentials. All pseudopotentials are listed with their recommended energy cutoffs in the Supporting Information, as are the valence configurations of each europium pseudopotential.

Structure relaxation

Initial test runs used Quantum Espresso v.6.4.1 while final relaxation runs used v.7.0.[30–32] For final relaxations, the kinetic energy cutoff for wavefunctions was 952 eV (70 Ry), and the cutoff for charge density and potential was 6260 eV (460 Ry), both just above the highest recommended values among the pslibrary pseudopotentials. Structure relaxations used a Monkhorst-Pack **k**-point grid[33] initialized with a minimum of $500/n$ points (n = number of atoms in the cell) distributed in proportion to reciprocal lattice vector lengths. We required 5×10^{-5} eV/atom (3.7×10^{-6} Ry/atom) convergence for electronic relaxation, 5×10^{-4} eV/atom (3.7×10^{-5} Ry/atom) for ionic relaxation, 9.45×10^{-3} eV/Å/atom (3.7×10^{-4} Ry/a_0/atom) for forces on each atom, and 0.5 kbar pressure for cell parameters. The force convergence follows Quantum Espresso's default of 10× the ionic convergence. Similar convergence criteria have performed well for diverse chemical systems.[34] Calculations included spin-orbit coupling but not the magnetic moment of Eu^{3+}.

To quantify stability, we relaxed the appropriate elemental compounds (eg. $Eu_{(s)}$). We then calculated the formation enthalpy (ΔH_f) by subtracting the total energy (E_{tot}) of each constituent elemental compound from E_{tot} of the compound of interest, with every value normalized to the number of atoms (eg. Eq. 1).

$$\Delta H_{f,Cs_2NaEuF_6} = E_{tot,Cs_2NaEuF_6} - \frac{2}{10}E_{tot,Cs} - \frac{1}{10}E_{tot,Na} - \frac{1}{10}E_{tot,Eu} - \frac{6}{10}E_{tot,F} \quad (1)$$

Finally, we used the ΔH_f of the compound and its "competing" phases to calculate energy above hull (E_{hull}) values. Competing phases are those that are closest to a proposed compound by composition. If a competing phase has multiple known polymorphs, we considered every polymorph in our calculations. For our Eu^{2+} competing phases, we calculated the total energy with the $4f^7$ core pseudopotential and subtracted the $Eu_{(s)}$ energy also calculated with the $4f^7$ core pseudopotential to get ΔH_f, giving results consistent with published ΔH_f values (Table 1).

Table 1: Computed ΔH_f values best match experimental ones when the appropriate pseudopotential is used for the compound total energy and the europium metal total energy ($4f^6$ core for Eu^{3+} and $4f^7$ core for Eu^{2+}). All ΔH_f values are in eV/atom.

Compound	ΔH_f Expt.	ΔH_f $4f^6$	ΔH_f $4f^7$
EuI_2 (2+)	-1.836[35]	-1.189	-1.742
EuO (2+)	-3.057[36]	-2.492	-3.219
Eu_2O_3 (3+)	-3.446[36]	-3.629	-2.219
EuF_3 (3+)	-4.195[36]	-4.184	-3.042
$EuPO_4$ (3+)	-3.220[37]	-3.026	-2.511

Other calculated properties

We also calculated band structures with the pslibrary and Pseudo-Dojo pseudopotentials, using the SeeK-path conventions.[38] We used the "normal" level cutoffs recommended by Pseudo-Dojo. The two pseudopotential sets gave nearly identical band structures. Additionally, we calculated dielectric functions with a uniform **k**-point grid. Convergence tests were performed to ensure enough points were used, and in each case, $>8\times10^4/n$ (n =number of atoms in the cell) **k**-points were used. The dielectric function was used to calculate the optical extinction coefficient, k, which is directly proportional to the absorption coefficient, α.

Characterization Methods

We collected powder X-ray diffraction (XRD) data on a Bruker D8 Advance diffractometer with capillary geometry and Mo Kα radiation. We performed Rietveld refinements to XRD data with GSAS-II.[39] Magnetic susceptibility and magnetization were measured with a Quantum Design Magnetic Property Measurement System. We placed powder in a gel capsule mounted in a straw and used the DC measurement mode. To capture powder images and analyze chemical composition with energy dispersive X-ray spectroscopy (EDS), we spread a thin layer of powder on carbon tape and collected data with a ThermoFisher Axia ChemiSEM. We used a Nanophoton Raman 11 confocal microscope for room temperature photoluminescence (PL) emission spectra. The instrument has a 532 nm excitation wavelength, a 50 μm slit width, and a 0.17 nm spectral resolution. We collected ten emission spectra across a sample and, seeing no variation in peak intensities, averaged the spectra to reduce noise.

Results and Discussion

Pseudopotential tests

On four Eu^{3+} chemical systems, we compared results from the relativistic pslibrary pseudopotentials ($4f^6$ frozen-core Eu) to the scalar relativistic SSSP pseudopotentials ($4f^6$ valence Eu). As a reference demonstrating the impact of using a europium pseudopotential with the wrong number of core 4f electrons, we also relaxed each system using the $4f^7$ frozen-core pslibrary pseudopotential meant to model Eu^{2+}. The Eu_2O_3-Al_2O_3 system is plotted in Figure 1, and the other systems are in the Supporting Information. For the Eu $4f^6$ core set, each experimentally reported compound is on the convex hull except $Eu_4Al_2O_9$ (E_{hull} = 1.9 meV/atom), and two unrealistic Materials Project compounds, $Eu_2Al_4O_9$ and $EuAl_{11}O_{18}$ (ion-swapped $NdAl_{11}O_{18}$) are well above it. In contrast, the $4f^6$ valence set places the known compounds $Eu_3Al_5O_{12}$ and $EuAlO_3$ above the hull. Using the relativistic, $4f^6$ frozen-core pseudopotential best represented the experimental observations in all four systems, and as expected, the $4f^7$ core pseudopotential does poorly for the Eu^{3+} systems. Therefore, we used the pslibrary set with 4f electrons in the europium core for our relaxations.

Stable compounds

We obtained prediction results for 33 proposed structures with 19 unreported stoichiometric compositions along with results for 48 polymorphs of 35 competing phases. Likely because the initial ion substitution did not alter the original lattice parameters, several compounds struggled to converge without a change in initial parameters. To get a rough relaxation, we used the graph neural network interatomic potential M3GNet[40] to relax them to a better starting point. The affected compounds and their provenance were $Eu_2P_4O_{13}$ (mp-771342), $Eu_2P_4O_{13}$ (mp-772787), $EuNb_3O_9$ (mp-1173575), and $EuNb_3O_9$ (mp-1210059). Calculation results for every proposed and competing structure, as well as a CIF for each relaxed proposed structure, are in the Supporting Information. Several proposed structures were predicted to be stable. They are listed in Table 2 with their energy relative to the convex hull if it were constructed without them (E_{rel}), and their crystal structures are shown in the Supporting Information.

Several observations about the proposed compounds should be made before discussing synthesis attempts. Two iodide compounds were predicted to be stable, $Cs_3Eu_2I_9$ and Na_3EuI_6, but we did not attempt to synthesize them because there are no known Eu^{3+} iodides. EuI_3 has not been realized experimentally[41,42] as its hydrated phases decompose directly into EuI_2,[43,44] and it has an estimated formation enthalpy $\sim$0.6 eV/atom higher than that of EuI_2.[35,45,46] Also, while Na_3MI_6 has been synthesized for M=Sm, Gd, Tb, and Dy, Na_3EuI_6 is conspicuously absent.[47] Second, the quaternary fluoride Cs_2NaEuF_6 has a non-polar predicted europium site symmetry that should preclude observation of the $^5D_0 \rightarrow {}^7F_0$ transition; however, the composition's actual structure, if

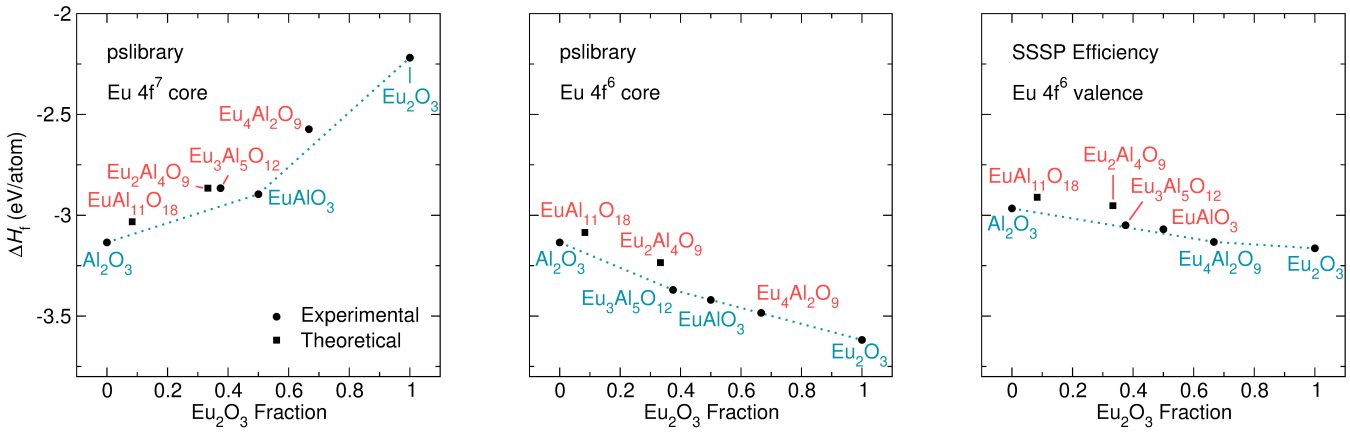

Figure 1: Three sets of pseudopotentials are tested on the Eu_2O_3-Al_2O_3 system. We assume that the binary oxides are stable. Blue compounds are on the calculated hull while red ones are not. Calculations using the set with $4f^6$ electrons in the Eu pseudopotential core best represent experimental observations.

Table 2: Compounds predicted to be stable ($E_{\text{hull}} = 0$) are listed along with their formation energy relative to the convex hull if it were constructed without them (E_{rel}). Also listed are the predicted symmetry and separation of their Eu^{3+} cations. Site symmetries followed by "(x)" are, in theory, not compatible with observing the $^5D_0 \rightarrow {}^7F_0$ transition.

Compound	E_{rel} (eV/atom)	Eu^{3+} Site Symmetry	Eu^{3+} Separation (Å)
$Cs_3Eu(PO_4)_2$	-0.057	C_1	5.42
$CsEuP_2O_7$	-0.035	C_1	5.59
Cs_2NaEuF_6	-0.033	O_h (x)	6.52
$Eu_2P_4O_{13}$	-0.023	C_1	4.02
$Na_7Eu_2(P_2O_7)_2(P_3O_{10})$	-0.005	C_1	5.48
Cs_5EuO_4	-0.003	C_1	6.15

synthesized, may of course be different. Finally, before completing the calculations, we were unaware of the prior report of $Eu_2P_4O_{13}$,[48] which is not in ICSD or the Materials Project. We calculated energies for four proposed polymorphs of the compound, and the most stable is the same as that realized experimentally. Only polycrystalline $Eu_2P_4O_{13}$ was previously synthesized by decomposition of $Eu(PO_3)_3$, so we did not pursue crystal growth here because of the complicated phase space. Figure 2 shows the absorption coefficient (13×13×13 **k**-point grid) and band structure of $Eu_2P_4O_{13}$. The compound has a direct band gap of 5.6 eV at the Γ point.

Synthesis of predicted compounds

We successfully synthesized polycrystalline Cs_2NaEuF_6. We first combined stoichiometric amounts of CsF (99.9%, Sigma Aldrich), EuF_3 (99.9%, Fisher), and NaF (99.99%, Alfa Aesar) under argon. We then placed them in a carbon-coated quartz tube before sealing the hygroscopic powder under vacuum. We heated the powder at 10°C/min to 600°C, held at that temperature for 4 h, and cooled back to room temperature at 10°C/min. The structure matched the cubic double perovskite structure type used in the DFT calculations (Figure 3). The XRD pattern is in Figure 4, and the refined atomic positions are in Table 3. The refined lattice parameter is $a = 9.1430(2)$ Å, smaller than the DFT predicted value of 9.2306 Å, and

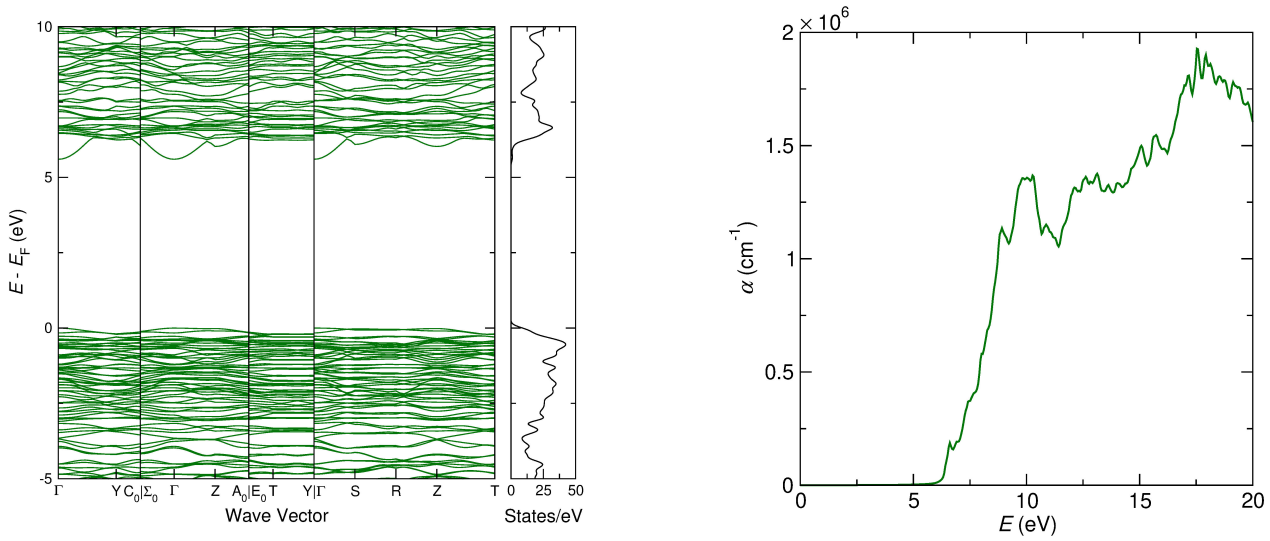

Figure 2: (Left) The band structure of $Eu_2P_4O_{13}$, calculated with the Pseudo-Dojo pseudopotential set, is plotted with the density of states. The direct band gap at the Γ point is 5.60 eV. (Right) The absorption coefficient of $Eu_2P_4O_{13}$ is plotted, and the first increase matches the calculated band gap.

the experimental Eu^{3+} separation is 6.47 Å. The XRD pattern did not change over two months, showing the fluoride's air stability (Supporting Information). A small $NaEuF_4$ impurity that we could not eliminate with excess CsF was present in each sample.

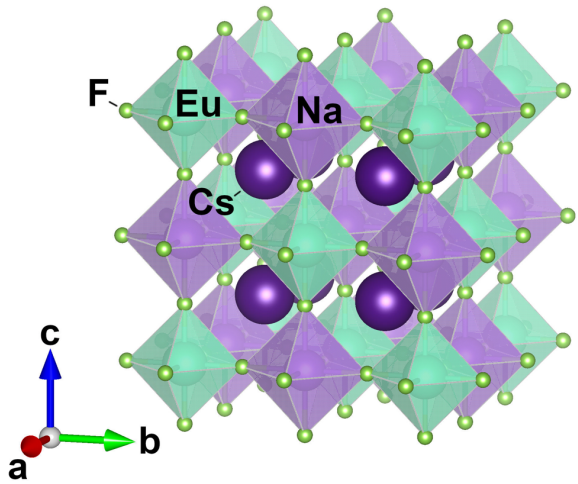

Figure 3: The double perovskite crystal structure of Cs_2NaEuF_6 is shown ($a = 9.1430$ Å). Cesium polyhedra are not shown to avoid crowding the image. NaF_6 octahedra are on the cell edges, and EuF_6 octahedra are on the cell faces and corners.

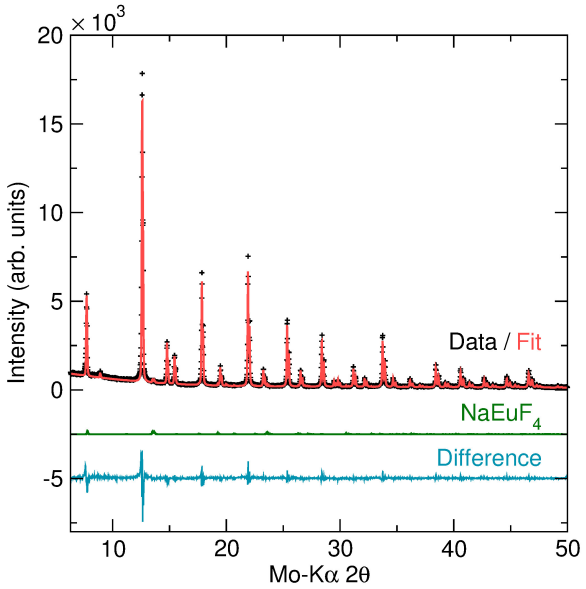

Figure 4: A powder XRD refinement of Cs_2NaEuF_6 is shown and includes a small $NaEuF_4$ impurity (1.7 wt%). Including Cs/Na site mixing did not improve the fit.

Table 3: The refined atomic positions for Cs_2NaEuF_6 are listed (space group $Fm\bar{3}m$, $a = 9.1430(2)$ Å).

Atom	Site	x	y	z
Cs	8c	0.25	0.25	0.25
Na	4b	0	0	0.5
Eu	4a	0	0	0
F	24e	0	0	0.248(1)

Next, we attempted to grow Cs_2NaEuF_6 single crystals by melting the starting powders in the carbon-coated tube and slow cooling through the melting point. As the melting point of the mixture is unknown, we attempted to heat the mixture to 700°C. At this temperature, though, the compound attacks the glass despite the carbon coating, eliminating that route to single crystals. Additionally, EuF_3 is insoluble in water, precluding simple solution precipitation. The most likely routes to high quality single crystals are a hydrofluoric acid solution method or a high-temperature sealed metal tube method.

To characterize the magnetic properties of Cs_2NaEuF_6, we collected field-cooled and zero-field-cooled magnetic susceptibility data from 2 to 395 K at 10 kOe on a 38.1 mg powder sample (Figure 5). The compound is a Van Vleck paramagnet, having a temperature-independent susceptibility at low temperature. The field-cooled and zero-field-cooled data did not deviate from each other. As observed in other Eu^{3+} compounds,[49] the data had a Curie tail near the base temperature due to Eu^{2+} impurities. Fitting to a Van Vleck model[49,50] above 55 K gives an energy separation between the $^7F_0$ and $^7F_1$ levels (λ) of 43.6 meV (λ/k_B = 506 K), which agrees with the PL emission spectrum discussed below. The corresponding magnetization curves are linear with no hysteresis, as expected for a paramagnet (Figure 5).

The calculated absorption coefficient (20×20×20 **k**-point grid) and band structure of Cs_2NaEuF_6 are Figure 6, showing a 6.9 eV band gap at the Γ point. Interestingly, the Cs_2NaEuF_6 polycrystalline product was gray instead of white. When the sealed tube contained starting powders in a boron nitride crucible and excess CsF in a separate crucible, the excess CsF also had a darker hue after synthesis. EDS revealed oxygen contamination in the perovskite product (Supporting Information). The gray hue, therefore, likely comes from the oxygen contamination or Eu^{2+} impurities, but no unidentified peaks were present in our XRD patterns.

On a Cs_2NaEuF_6 powder sample, we collected room temperature PL emission data (Figure 7). Because of the O_h site symmetry of Eu^{3+}, we would expect to observe only the $^5D_0 \rightarrow {}^7F_1$ transition with one peak.[51] Instead, we see each of the $^5D_0 \rightarrow {}^7F_J$ (J = 0-4) transitions, with one of three $J = 1$ peaks being the most intense. Many factors can lead to observing the additional transitions, including site disorder in the $NaEuF_4$ impurity,[52] oxygen or Eu^{2+} defects in the structure, or other defects. In the spectrum, the wavenumber shift between the observed $^5D_0 \rightarrow {}^7F_1$ and $^5D_0 \rightarrow {}^7F_0$ transitions is 365 cm^{-1} (45.3 meV), which is close to the 43.6 meV energy separation between the $^7F_0$ and $^7F_1$ levels calculated from magnetometry data.

We attempted several solid-state crystal growth methods for $Cs_3Eu(PO_4)_2$. The first followed a procedure for $Cs_3Ln(PO_4)_2$ (*Ln*: Y, Gd) that uses a Cs_2CO_3-H_3BO_3 flux.[53] After rinsing the flux off with water, we only recovered amorphous product. The second procedure adapted a $Rb_3Ln(PO_4)_2$ (*Ln*: Y, Dy–Lu) growth procedure[54] by using a eutectic Cs_2CO_3-CsF flux with $(NH_4)_2HPO_4$ and Eu_2O_3 in the stoichiometric ratio. After rinsing off the flux with water, only Eu_2O_3 remained. Additional details are in the Supporting Information.

To try to grow $CsEuP_2O_7$ crystals, we replaced the lanthanide precursor with europium compounds for several solution[55,56] and solid-state[57,58] synthesis procedures for isostructural lanthanide compounds. None of the procedures returned a phase containing Cs, Eu, P, and O. Both solid-state procedure products contained $EuPO_4$, with one including a small $EuPO_4$ crystal. The crystal's PL emission spectrum, with a

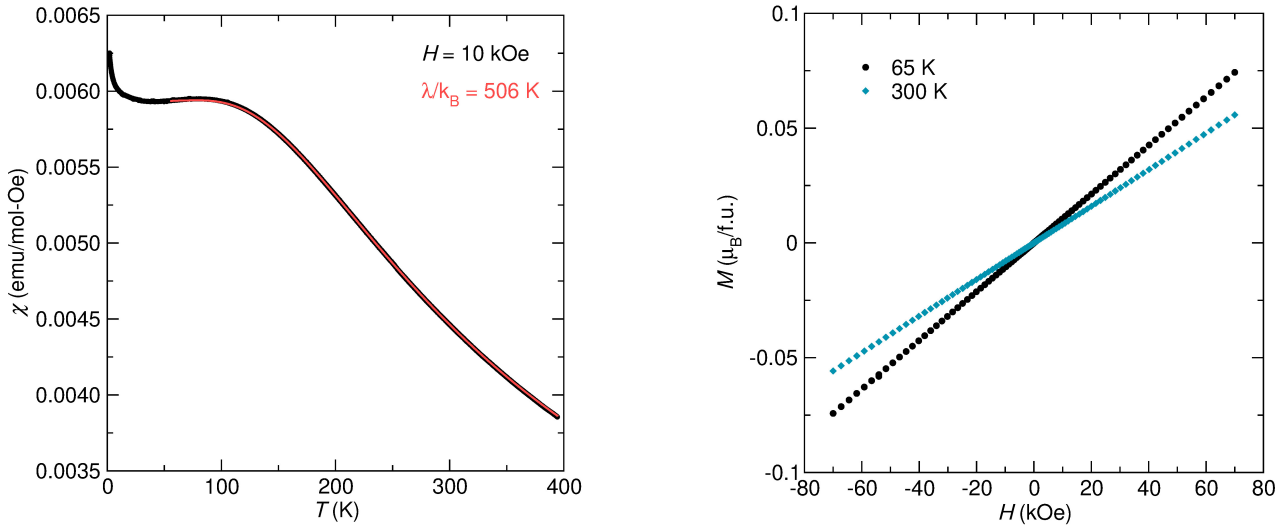

Figure 5: (Left) The field-cooled magnetic susceptibility of Cs_2NaEuF_6 is shown along with a Van Vleck susceptibility model fit. The data and fit show good agreement until near 55 K, where Eu^{2+} impurities create a Curie tail at lower temperatures. Data points are indistinguishable because of their tight spacing. (Right) The isothermal magnetization curves for paramagnetic Cs_2NaEuF_6 at 65 K and 300 K are linear and show no hysteresis.

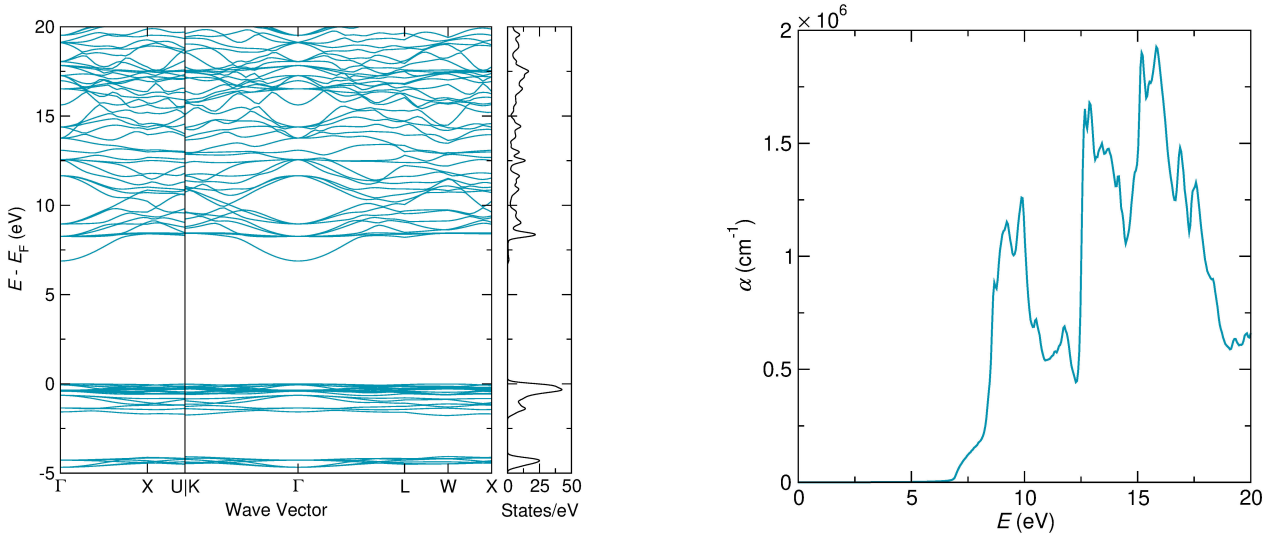

Figure 6: (Left) The band structure of Cs_2NaEuF_6, calculated with the Pseudo-Dojo pseudopotential set, is plotted with the density of states. The direct band gap at the Γ point is 6.88 eV. (Right) The absorption coefficient of Cs_2NaEuF_6 is plotted, and the first increase matches the calculated band gap.

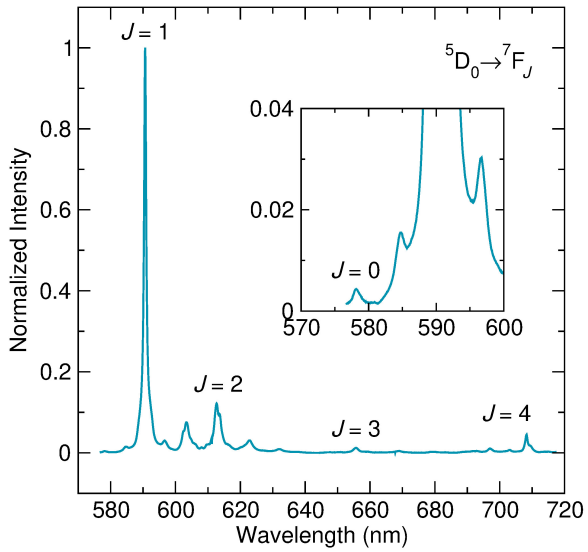

Figure 7: The room temperature PL emission spectrum of Cs_2NaEuF_6 shows each of the $^5D_0 \rightarrow ^7F_J$ (J = 0–4) transitions. The inset shows the weak $J = 0$ transition next to the much higher intensity $J = 1$ transition and its shoulder peaks.

sharp $^5D_0 \rightarrow ^7F_0$ transition matching a previous study[59] is in the Supporting Information along with additional synthesis attempt details.

For $Na_7Eu_2(P_2O_7)_2(P_3O_{10})$, we followed the procedure used for its only reported isostructural compound, $Na_7Y_2(P_2O_7)_2(P_3O_{10})$.[60] The resulting product also contained $EuPO_4$, along with an unidentifiable phase(s). The XRD pattern is in the Supporting Information along with synthesis attempt details. $EuPO_4$ again appears to be more energetically favorable than the predicted alkali-europium-phosphate compound.

Finally, we attempted to synthesize Cs_5EuO_4 by heating a stoichiometric mixture of Cs_2CO_3 and Eu_2O_3 in an alumina crucible. After 48 h at 1000°C, only Eu_2O_3 remained. We believe that Cs_2CO_3 decomposed to Cs_2O, which then evaporated since it was well above its melting point.

Other Materials Project database candidates

In addition to screening proposed candidates with DFT, we searched for existing entries in the Materials Project. First, using the database's API,[16] we queried every binary, ternary, and quaternary entry that contained the ions we used to propose structures. Then we filtered out entries with a Eu^{3+} minimum separation less than 3.95 Å and entries with non-polar Eu^{3+} site symmetries. After filtering, seven compounds remained, each experimentally realized. They are listed in Table 4. Their database IDs are in the Supporting Information, as are compounds with a smaller Eu^{3+} separation. Six of the seven are phosphates, which stems from our chemistry restrictions. Phosphorous, unlike the other cations, consistently forms polyatomic ions with oxygen. These polyatomic ions exist in various geometries (see extensive overviews[61–63]) that allow for large Eu^{3+} cation separation and provide space for the mononuclidic alkali metal cations Na^+ and Cs^+.

Encouragingly, six of the seven compounds have reported crystal growth procedures, and all seven compounds have reported $^5D_0 \rightarrow ^7F_0$ Eu^{3+} transitions: $CsEu(PO_3)_4$,[64,70] $NaEu(PO_3)_4$,[64,71] EuP_5O_{14},[65,66,72] $NaEuP_2O_7$,[71] $Eu(IO_3)_3$,[68,73,74] $Eu(PO_3)_3$,[69] and $EuPO_4$ (cf. Supporting Information).[59,75] For the Materials Project $Eu(PO_3)_3$ entry (space group $C222_1$), we could only find reports of polycrystalline samples.[48,69,76,77] However, single crystals are reported for a high temperature $Eu(PO_3)_3$ polymorph (space group $C2/c$) with a $^5D_0 \rightarrow ^7F_0$ active Eu^{3+} site symmetry (C_1) and a minimum Eu^{3+} separation of 5.30 Å.[48] Two of the phosphate candidates were studied together, showing a more intense $^5D_0 \rightarrow ^7F_0$ peak for $NaEuP_2O_7$ than for $NaEu(PO_3)_4$.[71] To our knowledge, only EuP_5O_{14} has a reported $^5D_0 \rightarrow ^7F_0$ inhomogeneous linewidth, 3.5 GHz, and optical coherence time, 10 μs.[78] Though much larger than needed to resolve hyperfine energy levels (∼70-140 MHz), this linewidth is similar to or lower than europium doped systems[79–82] while providing a drastically higher europium concentration.

Except for $NaEuP_2O_7$, each compound also has reported optical lifetimes for the $^5D_0$ energy level. The $^5D_0$ decay time of EuP_5O_{14}

Table 4: Listed are Materials Project entries (v2022.10.28) with Eu^{3+} separations ≥3.95 Å, the desired elements, and Eu^{3+} site symmetries compatible with observing the $^5D_0 \rightarrow {}^7F_0$ transition. For several lifetimes, the collection temperature is unclear.

Compound	MP E_{hull} (eV/atom)	Eu^{3+} Site Symmetry	MP Eu^{3+} Separation (Å)	$^5D_0$ Lifetime*
$CsEu(PO_3)_4$	0.021	C_1	5.85	∼3.2 μs** (77 K)[64]
$NaEu(PO_3)_4$	0.025	C_1	5.78	∼4.8 μs** (77 K)[64]
EuP_5O_{14}	0.019	C_1	5.16	4.4 ms (100 K),[65] 4.8 ms[66,67]
$NaEuP_2O_7$	0	C_1	4.34	-
$Eu(IO_3)_3$	0	C_1	4.31	1.6 ms (4.2 K)[68]
$Eu(PO_3)_3$ †	0	C_2	4.20	3.39 ms[69]
$EuPO_4$	0	C_1	4.05	∼0.81 ms[59]

*Values preceded by "∼" are estimated from graphs.
**See the main text note about reliability.
†See the main text about the high temperature polymorph with a larger Eu^{3+} separation.

is the largest at 4.8 ms.[66,67] The 3.39 ms lifetime for $Eu(PO_3)_3$, interestingly, increases for doped $(Y_{1-x}, Eu_x)(PO_3)_3$, indicating the 4.2 Å Eu^{3+} separation in the undoped sample leads to a high energy transfer probability.[69] Focusing on compounds with a Eu^{3+} separation >4.2 Å may therefore be prudent. The microsecond-scale lifetimes of $CsEu(PO_3)_4$ and $NaEu(PO_3)_4$ may be inaccurate as the report also lists a ∼4.4 μs lifetime for $KEu(PO_3)_4$ where others report 4.02 ms.[83]

In summary, each compound is a promising candidate. EuP_5O_{14} has benchmark values for its inhomogeneous linewidth and optical coherence time. $Eu(PO_3)_3$ and $Eu(IO_3)_3$ have millisecond-scale optical lifetimes. $EuPO_4$ and $NaEuP_2O_7$ have noticeable $^5D_0 \rightarrow {}^7F_0$ transitions at room temperature. And the $MEu(PO_3)_4$ compounds have large Eu^{3+} separation and may have longer than reported excited state lifetimes. $Eu(IO_3)_3$ has the additional advantage of avoiding phosphate chemistry, which can be plagued by synthesis complications related to producing crystals with the desired phosphate polyatomic ion.

Conclusions

We have explored several new stoichiometric candidates for optically addressable quantum memory systems that would not require isotopic enrichment and that have a large europium separation. We initially proposed 33 theoretical structures with 19 unrealized compositions. We then showed that using fully relativistic $4f^6$ and $4f^7$ frozen-core pseudopotentials for Eu^{3+} and Eu^{2+}, respectively, provide accurate predictions of europium system ΔH_f values. Using DFT calculations, we predicted that six of the unrealized compositions have a stable polymorph, including $Eu_2P_4O_{13}$, which, unknown to us beforehand, has been synthesized.

We then successfully synthesized the DFT-predicted compound Cs_2NaEuF_6, an air-stable and insulating double perovskite halide with a large Eu^{3+} separation that leads to paramagnetic behavior. Magnetic susceptibility, optical spectra, and EDS indicate that the compound contains several defects. Though our attempts to synthesize the other predicted compounds were unsuccessful, we believe more extensive tests are merited for $Cs_3Eu(PO_4)_2$ and $CsEuP_2O_7$ because of the compounds' favorable Eu^{3+} separations and site symmetries as well as the wide range of tunable synthesis parameters involved.

In addition to our predicted compounds, we evaluated Materials Project entries to find unexplored chemical spaces containing more stoichiometric candidates. Six known phosphate compounds and one iodate have large Eu^{3+} separations, appropriate Eu^{3+} site symmetries, and advantageous reported optical properties. The inhomogeneous linewidths of each, except EuP_5O_{14}, are unstudied.

To implement dense, optically addressable quantum memory with stoichiometric compounds, finding environmentally stable materials with controlled or minimal defect chemistry remains critical. The diversity of Eu^{3+} stoichiometric systems, though, necessitates data-driven approaches to finding promising candidates. This work demonstrates a pathway to accurate stability predictions and provides a new set of compounds to prioritize in future studies.

Acknowledgement We are grateful for helpful conversations with Elif Ertekin and André Schleife about our DFT procedures. DFT calculations were performed on the High Throughput Computing Pilot Program at the University of Illinois Urbana-Champaign. Optical characterization was performed at the Materials Research Laboratory Central Research Facilities at the University of Illinois. The authors acknowledge the use of facilities and instrumentation supported by NSF through the University of Illinois Materials Research Science and Engineering Center DMR-1720633. This work was supported by the U.S. Department of Energy, Office of Science, National Quantum Information Science Research Center Q-NEXT. Z.W.R. was supported by the National Science Foundation under Grant No. 1922758 (DIGI-MAT).

Supporting Information Available

The following Supporting Information is available free of charge at the ACS website:

Table S1. Relativistic pseudopotentials from the pslibrary v.1.0.0 set

Table S2. Scalar relativistic pseudopotentials from the SSSP Efficiency v.1.1.2 set

Table S3. Norm-conserving pseudopotentials from the Pseudo-Dojo standard accuracy sets

Table S4. Initial valence configurations of each Eu pseudopotential

Table S5. Proposed compound DFT results and structural information

Table S6. Competing compound DFT results and structural information

Table S7. Competing compounds and original structures associated with each proposed phase

Table S8. Materials Project entries with small Eu^{3+} separation

Table S9. Database IDs for Materials Project entries with large Eu^{3+} separation

Figures S1-S3. Additional pseudopotential test systems

Figure S4. Comparison of experimental and theoretical ΔH_f and cell volume values for competing phases

Figure S5. Crystal structures of the six DFT-predicted stable compounds

Figure S6. Band structures of Cs_2NaEuF_6 and $Eu_2P_4O_{13}$ calculated with pslibrary set pseudopotentials

Figure S7. XRD pattern stability of Cs_2NaEuF_6 over two months

Figure S8. SEM images of Cs_2NaEuF_6 powder used for EDS data collection

Figure S9. EDS spectra of a Cs_2NaEuF_6 powder sample

Figures S10-S12, S14. XRD refinements of products from unsuccessful synthesis procedures for DFT-predicted compounds

Figure S13. PL emission spectrum of a $EuPO_4$ crystal

References

(1) Könz, F.; Sun, Y.; Thiel, C.; Cone, R.; Equall, R.; Hutcheson, R.; Macfarlane, R. Temperature and concentration dependence of optical dephasing, spectral-hole lifetime, and anisotropic absorption in Eu^{3+}:Y_2SiO_5. *Physical Review B* **2003**, *68*, 085109.

(2) Longdell, J. J.; Fraval, E.; Sellars, M. J.; Manson, N. B. Stopped light with storage times greater than one second using

electromagnetically induced transparency in a solid. *Physical Review Letters* **2005**, *95*, 063601.

(3) Böttger, T.; Thiel, C.; Cone, R.; Sun, Y. Effects of magnetic field orientation on optical decoherence in Er^{3+}:Y_2SiO_5. *Physical Review B* **2009**, *79*, 115104.

(4) Zhong, M.; Hedges, M. P.; Ahlefeldt, R. L.; Bartholomew, J. G.; Beavan, S. E.; Wittig, S. M.; Longdell, J. J.; Sellars, M. J. Optically addressable nuclear spins in a solid with a six-hour coherence time. *Nature* **2015**, *517*, 177–180.

(5) Ahlefeldt, R. L.; Pearce, M. J.; Hush, M. R.; Sellars, M. J. Quantum processing with ensembles of rare-earth ions in a stoichiometric crystal. *Physical Review A* **2020**, *101*, 012309.

(6) Ahlefeldt, R. L.; Smith, A.; Sellars, M. J. Ligand isotope structure of the optical $^7F_0 \rightarrow ^5D_0$ transition in $EuCl_3 \cdot 6H_2O$. *Physical Review B* **2009**, *80*, 205106.

(7) Ahlefeldt, R. L.; Manson, N. B.; Sellars, M. J. Optical lifetime and linewidth studies of the $^7F_0 \rightarrow ^5D_0$ transition in $EuCl_3 \cdot 6H_2O$: A potential material for quantum memory applications. *Journal of Luminescence* **2013**, *133*, 152–156.

(8) Ahlefeldt, R. L.; McAuslan, D. L.; Longdell, J. J.; Manson, N. B.; Sellars, M. J. Precision Measurement of Electronic Ion-Ion Interactions between Neighboring Eu^{3+} Optical Centers. *Physical Review Letters* **2013**, *111*, 240501.

(9) Ahlefeldt, R.; Hush, M. R.; Sellars, M. Ultranarrow optical inhomogeneous linewidth in a stoichiometric rare-earth crystal. *Physical Review Letters* **2016**, *117*, 250504.

(10) Dal Corso, A. Pseudopotentials periodic table: From H to Pu. *Computational Materials Science* **2014**, *95*, 337–350.

(11) Gao, M. C.; Rollett, A. D.; Widom, M. Lattice stability of aluminum-rare earth binary systems: A first-principles approach. *Physical Review B* **2007**, *75*, 174120.

(12) Ong, S. P.; Richards, W. D.; Jain, A.; Hautier, G.; Kocher, M.; Cholia, S.; Gunter, D.; Chevrier, V. L.; Persson, K. A.; Ceder, G. Python Materials Genomics (pymatgen): A robust, open-source python library for materials analysis. *Computational Materials Science* **2013**, *68*, 314–319.

(13) Hautier, G.; Fischer, C.; Ehrlacher, V.; Jain, A.; Ceder, G. Data mined ionic substitutions for the discovery of new compounds. *Inorganic Chemistry* **2011**, *50*, 656–663.

(14) Belsky, A.; Hellenbrandt, M.; Karen, V. L.; Luksch, P. New developments in the Inorganic Crystal Structure Database (ICSD): accessibility in support of materials research and design. *Acta Crystallographica Section B* **2002**, *58*, 364–369.

(15) Jain, A.; Ong, S. P.; Hautier, G.; Chen, W.; Richards, W. D.; Dacek, S.; Cholia, S.; Gunter, D.; Skinner, D.; Ceder, G., et al. Commentary: The Materials Project: A materials genome approach to accelerating materials innovation. *APL Materials* **2013**, *1*, 011002.

(16) Ong, S. P.; Cholia, S.; Jain, A.; Brafman, M.; Gunter, D.; Ceder, G.; Persson, K. A. The Materials Application Programming Interface (API): A simple, flexible and efficient API for materials data based on REpresentational State Transfer (REST) principles. *Computational Materials Science* **2015**, *97*, 209–215.

(17) Fedorov, P. P. Systems of alkali and rare-earth metal fluorides. *Zhurnal Neorganicheskoj Khimii* **1999**, *44*, 1792–1818.

(18) Turkoglu, O.; Soylak, M.; Belenli, I. Synthesis and characterization of β type

solid solution in the binary system of Bi_2O_3-Eu_2O_3. *Bulletin of Materials Science* **2002**, *25*, 583–588.

(19) Saha, S.; Chanda, S.; Dutta, A.; Kumar, U.; Ranjan, R.; Sinha, T. P. Dielectric relaxation and anti-ferromagnetic coupling of $BiEuO_3$ and $BiGdO_3$. *Journal of Magnetism and Magnetic Materials* **2014**, *360*, 80–86.

(20) Andrievskaya, E. R.; Zaitseva, Z. A.; Shevchenko, A. V.; Lopato, L. M. Phase diagram of the Eu_2O_3-Y_2O_3 system. *Inorganic Materials* **1997**, *33*, 390–393.

(21) Mizuno, M.; Yamada, T.; Noguchi, T. Phase diagrams of the systems Al_2O_3-Eu_2O_3 and Al_2O_3-Gd_2O_3 at high temperatures. *Yogyo-Kyokai-Shi* **1977**, *85*, 374–9.

(22) Wu, P.; Pelton, A. D. Coupled thermodynamic-phase diagram assessment of the rare earth oxide-aluminium oxide binary systems. *Journal of Alloys and Compounds* **1992**, *179*, 259–287.

(23) Lejaeghere, K.; Bihlmayer, G.; Björkman, T.; Blaha, P.; Blügel, S.; Blum, V.; Caliste, D.; Castelli, I. E.; Clark, S. J.; Dal Corso, A., et al. Reproducibility in density functional theory calculations of solids. *Science* **2016**, *351*, aad3000.

(24) Prandini, G.; Marrazzo, A.; Castelli, I. E.; Mounet, N.; Marzari, N. Precision and efficiency in solid-state pseudopotential calculations. *npj Computational Materials* **2018**, *4*, 1–13.

(25) Prandini, G.; Marrazzo, A.; Castelli, I. E.; Mounet, N.; Passaro, E.; Marzari, N. A Standard Solid State Pseudopotentials (SSSP) library optimized for precision and efficiency. 2021; `https://doi.org/10.24435/materialscloud:rz-77`.

(26) Koelling, D. D.; Harmon, B. N. A technique for relativistic spin-polarised calculations. *Journal of Physics C: Solid State Physics* **1977**, *10*, 3107.

(27) Gollisch, H.; Fritsche, L. Relativistic one-particle equation for electron states of heavy metals. *physica status solidi (b)* **1978**, *86*, 145–150.

(28) Takeda, T. The scalar relativistic approximation. *Zeitschrift für Physik B Condensed Matter* **1978**, *32*, 43–48.

(29) van Setten, M. J.; Giantomassi, M.; Bousquet, E.; Verstraete, M. J.; Hamann, D. R.; Gonze, X.; Rignanese, G.-M. The PseudoDojo: Training and grading a 85 element optimized norm-conserving pseudopotential table. *Computer Physics Communications* **2018**, *226*, 39–54.

(30) Giannozzi, P. et al. QUANTUM ESPRESSO: a modular and open-source software project for quantum simulations of materials. *Journal of Physics: Condensed Matter* **2009**, *21*, 395502.

(31) Giannozzi, P.; Andreussi, O.; Brumme, T.; Bunau, O.; Nardelli, M. B.; Calandra, M.; Car, R.; Cavazzoni, C.; Ceresoli, D.; Cococcioni, M., et al. Advanced capabilities for materials modelling with Quantum ESPRESSO. *Journal of Physics: Condensed Matter* **2017**, *29*, 465901.

(32) Giannozzi, P.; Baseggio, O.; Bonfà, P.; Brunato, D.; Car, R.; Carnimeo, I.; Cavazzoni, C.; De Gironcoli, S.; Delugas, P.; Ferrari Ruffino, F., et al. Quantum ESPRESSO toward the exascale. *The Journal of Chemical Physics* **2020**, *152*, 154105.

(33) Monkhorst, H. J.; Pack, J. D. Special points for Brillouin-zone integrations. *Physical Review B* **1976**, *13*, 5188.

(34) Jain, A.; Hautier, G.; Moore, C. J.; Ong, S. P.; Fischer, C. C.; Mueller, T.; Persson, K. A.; Ceder, G. A high-throughput infrastructure for density functional theory calculations. *Computational Materials Science* **2011**, *50*, 2295–2310.

(35) Wicks, C. E.; Block, F. E. *Thermodynamic properties of 65 elements: their oxides, halides, carbides and nitrides*; US Government Printing Office, 1963; Vol. 605.

(36) Kubaschewski, O., Ed. *Materials Thermochemistry, 6th ed.*; Pergamon Press: New York, 1993.

(37) Popa, K.; Konings, R. J. M. High-temperature heat capacities of $EuPO_4$ and $SmPO_4$ synthetic monazites. *Thermochimica Acta* **2006**, *445*, 49–52.

(38) Hinuma, Y.; Pizzi, G.; Kumagai, Y.; Oba, F.; Tanaka, I. Band structure diagram paths based on crystallography. *Computational Materials Science* **2017**, *128*, 140–184.

(39) Toby, B. H.; Von Dreele, R. B. GSAS-II: the genesis of a modern open-source all purpose crystallography software package. *Journal of Applied Crystallography* **2013**, *46*, 544–549.

(40) Chen, C.; Ong, S. P. A universal graph deep learning interatomic potential for the periodic table. *Nature Computational Science* **2022**, *2*, 718–728.

(41) Asprey, L. B.; Keenan, T. K.; Kruse, F. H. Preparation and crystal data for lanthanide and actinide triiodides. *Inorganic Chemistry* **1964**, *3*, 1137–1141.

(42) Wetzel, K. In *Handbook of Preparative Inorganic Chemistry*; Brauer, G., Ed.; Academic Press: New York, 1963; p 1150.

(43) Jenden, C. M.; Lyle, S. J. A Mössbauer spectroscopic study of the iodides of europium. *Journal of the Chemical Society, Dalton Transactions* **1982**, 2409–2414.

(44) Chengpeng, D.; Jinqiu, Y.; Hongwei, L.; Peng, P.; Hao, W.; Huaqiang, H.; Shihong, Y.; Yunsheng, H. Ammonium-iodide route to anhydrous EuI_2: mechanism and preparation. *Journal of Rare Earths* **2015**, *33*, 1189–1195.

(45) Kirklin, S.; Saal, J. E.; Meredig, B.; Thompson, A.; Doak, J. W.; Aykol, M.; Rühl, S.; Wolverton, C. The Open Quantum Materials Database (OQMD): assessing the accuracy of DFT formation energies. *npj Computational Materials* **2015**, *1*, 1–15.

(46) Meyer, G. Small cause–Great effect: What the $4f^{n+1}5d^0 \rightarrow 4f^n5d^1$ configuration crossover does to the chemistry of divalent rare-earth halides and coordination compounds. *Journal of Solid State Chemistry* **2019**, *270*, 324–334.

(47) Bohnsack, A.; Meyer, G. Ternäre Halogenide vom Typ A_3MX_6. V. Synthese, Kristallstrukturen und Natrium-Ionenleitfähigkeit der ternären Iodide Na_3MI_6 (M = Sm, Gd–Dy) sowie der Mischkristalle $Na_3GdBr_{6-x}I_x$. *Zeitschrift für anorganische und allgemeine Chemie* **1997**, *623*, 837–843.

(48) Grunwald, W.; Wittich, K.; Glaum, R. Anhydrous Europium Phosphates: A Comprehensive Report on Syntheses, Crystal Structures, and Phase Relations. *Zeitschrift für Anorganische und Allgemeine Chemie* **2018**, *644*, 1403–1414.

(49) Takikawa, Y.; Ebisu, S.; Nagata, S. Van Vleck paramagnetism of the trivalent Eu ions. *Journal of Physics and Chemistry of Solids* **2010**, *71*, 1592–1598.

(50) Van Vleck, J. H. *The Theory Of Electric And Magnetic Susceptibilities*; Oxford University Press, 1932; pp 245–249.

(51) Tanner, P. A. Some misconceptions concerning the electronic spectra of tripositive europium and cerium. *Chemical Society Reviews* **2013**, *42*, 5090–5101.

(52) Zakaria, D.; Mahiou, R.; Avignant, D.; Zahir, M. Single-crystal structure refinement and luminescence analysis of β-$NaEuF_4$. *Journal of Alloys and Compounds* **1997**, *257*, 65–68.

(53) Wang, Y.; Lian, Z.; Su, X.; Yang, Z.; Pan, S.; Yan, Q.; Zhang, F. $Cs_6RE_2(PO_4)_4$ (RE = Y and Gd): two new members of the alkali rare-earth double phosphates. *New Journal of Chemistry* **2015**, *39*, 4328–4333.

(54) Tisdale, H. B.; Christian, M. S.; Morrison, G.; Besmann, T. M.; Sun, K.; Was, G. S.; zur Loye, H.-C. Investigation of Rare Earth-Containing Double Phosphates of the Type $A_3Ln(PO_4)_2$ (Ln= Y, La, Pr, Nd, and Sm–Lu) as Potential Nuclear Waste Forms. *Chemistry of Materials* **2022**, *34*, 3819–3830.

(55) Essehli, R.; El Bali, B.; Dusek, M.; Fejfarova, K.; Lachkar, M. Yttrium hydrogendiphosphate trihydrate. *Acta Crystallographica Section E: Structure Reports Online* **2007**, *63*, i80–i82.

(56) Essehli, R.; Lamhamdi, A.; Alaoui, A. T.; El Bali, B.; Mejdoubi, E.; Lachkar, M.; Dusek, M.; Fejfarova, K. $AErP_2O_7$ (A = Rb, Cs) and $HEuP_2O_7{\cdot}3H_2O$: Crystal Structures, Vibrational Studies and Thermal Behaviours. *Journal of Chemical Crystallography* **2012**, *42*, 475–485.

(57) Mbarek, A. Synthesis, structural and optical properties of Eu^{3+}-doped $ALnP_2O_7$ (A = Cs, Rb, Tl; Ln= Y, Lu, Tm) pyrophosphates phosphors for solid-state lighting. *Journal of Molecular Structure* **2017**, *1138*, 149–154.

(58) Zhao, D.; Ma, F.; Zhang, R.; Zhang, R.; Zhang, L.; Fan, Y. Crystal structure and luminescence properties of self-activated phosphor $CsDyP_2O_7$. *Materials Research Bulletin* **2017**, *87*, 202–207.

(59) Chen, G.; Hölsä, J.; Peterson, J. A luminescence study of single-crystal $EuPO_4$ at high pressure. *Journal of Physics and Chemistry of Solids* **1997**, *58*, 2031–2037.

(60) Hamady, A.; Jouini, T. $Na_7Y_2(P_2O_7)_2(P_3O_{10})$ – a new layer and tunnel structure. *Zeitschrift für anorganische und allgemeine Chemie* **1996**, *622*, 1987–1990.

(61) Averbuch-Pouchot, M.; Durif, A. Crystal Chemistry of Oligophosphates. *Annual Review of Materials Science* **1991**, *21*, 65–92.

(62) Durif, A. *Crystal Chemistry of Condensed Phosphates*; Springer Science & Business Media, 1995.

(63) Attfield, J. P. *Encyclopedia of Inorganic and Bioinorganic Chemistry*; John Wiley & Sons, Ltd, 2014; pp 1–16.

(64) Barsukov, I. V.; Syt'ko, V. V.; Umreiko, D. S. Influence of the structure of the $MEu(PO_3)_4$ crystals on their luminescent properties. *Journal of Applied Spectroscopy* **2004**, *71*, 676–680.

(65) Brecher, C. Europium in the ultraphosphate lattice: Polarized spectra and structure of EuP_5O_{14}. *The Journal of Chemical Physics* **1974**, *61*, 2297–2315.

(66) Blanzat, B.; Denis, J.-P.; Loriers, J. Luminescence, structural properties and energy transfer mechanisms in some rare earth ultraphosphates. Proceedings of the Tenth Rare Earth Research Conference. 1973; pp 1170–1177.

(67) Blanzat, B.; Boehm, L.; Jørgensen, C.; Reisfeld, R.; Spector, N. Transition probabilities of europium (III) in zirconium and beryllium fluoride glasses, phosphate glass, and pentaphosphate crystals. *Journal of Solid State Chemistry* **1980**, *32*, 185–192.

(68) van Vliet, J. P. M.; Blasse, G.; Brixner, L. H. Luminescence properties of the system $Gd_{1-x}Eu_x(IO_3)_3$. *Journal of the Electrochemical Society* **1988**, *135*, 1574.

(69) Zhang, X.; Chen, P.; Wang, Z.; Zhou, L.; Zhou, F. Structure and spectroscopic properties of (Y, Eu)$(PO_3)_3$ polyphosphate red phosphors. *Solid State Sciences* **2016**, *58*, 80–85.

(70) Zhu, J.; Cheng, W.-D.; Zhang, H. Caesium europium (III) polyphosphate, $CsEu(PO_3)_4$. *Acta Crystallographica Section E* **2009**, *65*, i70–i70.

(71) Zhu, J.; Cheng, W.-D.; Wu, D.-S.; Zhang, H.; Gong, Y.-J.; Tong, H.-N.; Zhao, D. Crystal and band structures, and optical characterizations of sodium rare earth phosphates $NaLnP_2O_7$ and $NaLn(PO_3)_4$ (Ln= Ce, Eu). *Journal of Alloys and Compounds* **2008**, *454*, 419–426.

(72) Sekita, M.; Minami, F.; Okamoto, E.; Masui, H. Optical Spectra of EuP_5O_{14} between 77 and 583 K. *physica status solidi (b)* **1980**, *101*, 353–361.

(73) Phanon, D.; Mosset, A.; Gautier-Luneau, I. New iodate materials as potential laser matrices. Preparation and characterisation of α-$M(IO_3)_3$ (M=Y, Dy) and β-$M(IO_3)_3$ (M=Y, Ce, Pr, Nd, Eu, Gd, Tb, Dy, Ho, Er). Structural evolution as a function of the Ln^{3+} cationic radius. *Solid State Sciences* **2007**, *9*, 496–505.

(74) Xu, W.; Xu, H.; Wang, S.; Wang, Z.; Xu, X.; Zhang, X.; Wu, S. Scintillation materials based on metal iodates by rare earth doping modifications for use in radioluminescence and X-ray imaging. *CrystEngComm* **2021**, *23*, 4103–4108.

(75) Ushakov, S. V.; Helean, K. B.; Navrotsky, A.; Boatner, L. A. Thermochemistry of rare-earth orthophosphates. *Journal of Materials Research* **2001**, *16*, 2623–2633.

(76) Cannas, M.; Manca, E.; Pinna, G.; Bettinelli, M.; Speghini, A. Structural investigation of amorphous europium metaphosphate by X-ray diffraction. *Zeitschrift für Naturforschung A* **1998**, *53*, 919–927.

(77) Buijs, M.; Blasse, G. One-and three-dimensional energy migration in dimorphic EuP_3O_9. *Journal of Luminescence* **1988**, *39*, 323–334.

(78) Shelby, R. M.; Macfarlane, R. M. Frequency-Dependent Optical Dephasing in the Stoichiometric Material EuP_5O_{14}. *Physical Review Letters* **1980**, *45*, 1098.

(79) Flinn, G. P.; Jang, K. W.; Ganem, J.; Jones, M. L.; Meltzer, R. S.; Macfarlane, R. M. Sample-dependent optical dephasing in bulk crystalline samples of Y_2O_3:Eu^{3+}. *Physical Review B* **1994**, *49*, 5821.

(80) Sellars, M. J.; Fraval, E.; Longdell, J. J. Investigation of static electric dipole–dipole coupling induced optical inhomogeneous broadening in Eu^{3+}:Y_2SiO_5. *Journal of Luminescence* **2004**, *107*, 150–154.

(81) Bartholomew, J. G.; Zhang, Z.; Di Lieto, A.; Tonelli, M.; Goldner, P. High resolution spectroscopy of the $^7F_0 \leftrightarrow {}^5D_0$ transition in Eu^{3+}:KYF_4. *Journal of Luminescence* **2016**, *171*, 221–225.

(82) Casabone, B.; Benedikter, J.; Hümmer, T.; Oehl, F.; Lima, K. d. O.; Hänsch, T. W.; Ferrier, A.; Goldner, P.; Riedmatten, H. d.; Hunger, D. Cavity-enhanced spectroscopy of a few-ion ensemble in Eu^{3+}:Y_2O_3. *New Journal of Physics* **2018**, *20*, 095006.

(83) Malinowski, M.; Kaczkan, M. Absorption intensity analysis and emission properties $KEu(PO_3)_4$ and $KEu_xY_{1-x}(PO_3)_4$ crystals. *Journal of Luminescence* **2019**, *211*, 138–143.

TOC Graphic